AGU PUBLICATIONS

Geophysical Research Letters

RESEARCH LETTER
10.1002/2013GL058646

Key Points:
- Midlatitude information pathways weaken and shift poleward as the climate warms.
- Major tropical information pathways start diminishing.
- Averaged over the Northern Hemisphere, the atmospheric information flow weakens.

Supporting Information:
- Readme
- Figure S1

Correspondence to:
Yi Deng,
yi.deng@eas.gatech.edu

Citation:
Deng, Y., and I. Ebert-Uphoff (2014), Weakening of atmospheric information flow in a warming climate in the Community Climate System Model, *Geophys. Res. Lett.*, *41*, doi:10.1002/2013GL058646.

Received 8 NOV 2013
Accepted 20 DEC 2013
Accepted article online 26 DEC 2013

Weakening of atmospheric information flow in a warming climate in the Community Climate System Model

Yi Deng[1] and Imme Ebert-Uphoff[2]

[1]School of Earth and Atmospheric Sciences, Georgia Institute of Technology, Atlanta, Georgia, USA, [2]Electrical and Computer Engineering, Colorado State University, Fort Collins, Colorado, USA

Abstract We introduce a new perspective of climate change by revealing the changing characteristics of atmospheric information flow in a warming climate. The key idea is to interpret large-scale atmospheric dynamical processes as information flow around the globe and to identify the pathways of this information flow using a climate network based on causal discovery and graphical models. We construct such networks using the daily geopotential height data from the Community Climate System Model Version 4.0 (CCSM4.0)'s 20th century climate simulation and 21st century climate projection. We show that in the CCSM4.0 model under enhanced greenhouse gases (GHGs) forcing, prominent midlatitude information pathways in the midtroposphere weaken and shift poleward, while major tropical information pathways start diminishing. Averaged over the entire Northern Hemisphere, the atmospheric information flow weakens. The implications of this weakening for the interconnectivity among different geographical locations and for the intrinsic predictability of the atmosphere are discussed.

1. Climate Networks Based on Causal Discovery

The traditional idea of climate networks is to define a correlation network of nodes where each node represents a point on a global grid [*Tsonis and Roebber*, 2004]. Any two nodes are connected if the correlation of a specific atmospheric and/or oceanic variable measured at the two nodes is beyond a threshold [*Tsonis and Roebber*, 2004; *Tsonis et al*., 2006]. The introduction of a climate network effectively brought the vast framework of network analysis to climate science and triggered a flurry of research activity in this area, including classification of network type, analysis of network properties such as density of connections, backbone of the network, and effects of natural modes of climate variability (e.g., El Niño) on network properties [*Tsonis et al*., 2007; *Tsonis and Swanson*, 2008; *Gozolchiani et al*., 2008; *Yamasaki et al*., 2008; *Donges et al*., 2009; *Steinhaeuser et al*., 2010]. While correlation networks remain the most common type, three more definitions have recently been proposed. MI networks [*Donges et al*., 2009] use mutual information, rather than correlation, to decide whether two nodes should be connected. Phase synchronization networks [*Yamasaki et al*., 2009] use the level of robust phase synchronization between nodes as criterion for connections, and event synchronization networks [*Boers et al*., 2013] focus on the level of synchronization of extreme events (maxima and minima) in the nodes' time series. While correlation and MI networks emphasize instantaneous connections, synchronization networks focus on connections over time by considering temporal lags. All of the above network definitions, however, decide whether an edge exists between two nodes, X and Y, in the network based only on a test involving those two nodes. Thus, they do not truly distinguish between direct and indirect causal connections. Furthermore, the results for many of them have been described as being fairly similar to correlation networks, especially for MI networks and phase synchronization networks [*Yamasaki et al*., 2009].

We recently introduced a very different type of climate network based on causal discovery theory [*Ebert-Uphoff and Deng*, 2010, 2012a, 2012b]. *Hlinka et al*. [2013] also explore causal-discovery-based methods for climate networks, contrasting methods based on Granger causality and on transfer entropy [*Runge et al*., 2012]. The motivation behind the introduction of causal-discovery-based climate networks is to interpret large-scale atmospheric dynamical processes as information transmission around the globe and to identify the most critical information transmission pathways across various timescales. Causal discovery theory seeks to learn causal relationships from observational data and has found applications in

many areas including bioinformatics and economics. Specifically, we use structure learning for probabilistic graphical models for which efficient algorithms were developed already in the late 1980s [*Pearl*, 1988; *Spirtes et al*., 1993]. The key idea of these algorithms is to start with a fully connected network and to use *conditional* independence tests to eliminate *indirect* connections between network nodes. When deciding whether an edge between nodes *X* and *Y* should be deleted, the full context of the surrounding network is taken into account through the use of a conditioning set, *S*, which represents all nodes that could possibly have an influence on *X* and *Y*. The challenge of these algorithms is to implement these tests in an efficient way to keep the computational complexity manageable. A simple, yet powerful, algorithm for this purpose is the Peter and Clark (PC) algorithm [*Spirtes and Glymour*, 1991], which is employed in our study (see supporting information for a more detailed description). The type of graphical model we use is a directed graph, also known as Bayesian network. Each node in such a network represents an observed variable and the existence of an edge between two nodes indicates statistical dependency between two nodes. The resulting network can then be interpreted as causal models, i.e., each edge $X \rightarrow Y$ in the network indicates that a variable *X* is likely to have a causal effect on variable *Y*, which is analogous to saying that there is *information flow* from *X* to *Y*.

As a result of the consideration of the conditional independence, networks obtained through causal discovery take longer to calculate than correlation networks, but have drastically fewer edges and the edges have a very different meaning. While correlation-type networks are well suited to identify *similarities* between locations *X* and *Y*, the new type of climate network reveals the existence of *information pathways*, if any, between *X* and *Y*. In *Ebert-Uphoff and Deng* [2012b], we built such networks with daily geopotential height data at 500 hPa level and the network thus operates on a very different time scale than correlation networks where monthly data are often used. The result is a *temporal* directed graph that tracks the interactions at individual geographical locations over the time span of about 14 days. An *edge* in the resulting graph represents strong information flow from one specific location to a second location over a specified number of days, e.g., from some location *A* to some location *B* with the signal traveling for, say, two days to reach *B* (see Step 5 of section 2 for a more detailed description).

In this study, for the first time we apply the concept of causal-discovery-based climate networks to understand *climate change*. As an initial step, we focus in our analysis on a single climate model — the National Center for Atmospheric Research (NCAR) Community Climate System Model Version 4.0 (CCSM4.0) [*Gent et al*., 2011] and consider a specific future emission scenario — Representative Concentration Pathway 8.5 (RCP8.5), which assumes that the total radiative forcing due to anthropogenic greenhouse gases (GHGs) reaches 8.5 Wm^{-2} by 2100 [*Van Vuuren et al*., 2011]. To learn about the changing characteristics of atmospheric information flow in a warming climate in this model, we develop and compare causal-discovery-based climate networks using output data from the CCSM4.0's 20th century climate simulation and 21st century climate projection. Specifically, we focus our initial investigation on the change of the atmospheric information flow at the midtropospheric level of 500 hPa in boreal winter. The choice of the 500 hPa level is due to the fact that tracking propagation of large-scale atmospheric disturbances (e.g., in terms of vorticity anomalies) at this particular level often provides most critical information about local weather change and the first successful numerical weather prediction was also carried out in 1950 by integrating the so-called barotropic vorticity equation on 500 hPa level [*Charney et al*., 1950].

2. Data and Methods

The data used in this study is the 50 year, 500 hPa geopotential height record from three different sources. These are: (1) NCEP/NCAR reanalysis (observation) for years 1950–2000 [*Kalnay et al*., 1996; *Kistler et al*., 2001], (2) NCAR CCSM4.0 model's 20th century climate simulation for years 1950–2000, and (3) CCSM4.0 model's future climate projection (21st century climate simulation) under RCP8.5 scenario for years 2050–2100. Geopotential height is used here since many atmospheric fields such as winds, vorticity, and lower tropospheric temperature can be approximately inferred from the geopotential height field due to the geostrophic and hydrostatic balance of the extratropical large-scale atmospheric flow [e.g., *Holton and Hakim*, 2012]. For each of the three data sets we use the daily data for the boreal winter (Dec–Jan–Feb) and follow the method described by *Ebert-Uphoff and Deng* [2012a, 2012b] to develop climate networks based on causal discovery theory. The steps are as follows:

1. We define a set of N grid points equally spaced around the globe and interpolate/extrapolate geopotential height data onto this grid. We currently use $N = 200$ grid points due to the computational complexity of Step 3, but plan to increase the number in the future. Since there is no closed-form solution for generating such an equally spaced grid, we use an approximate method instead [*Bendito et al*., 2007]. To check for grid variability we generate three grids and calculate all of our results for all three grids.
2. Next we choose a time span over which we want to develop the model, in our case $S = 15$ slices, with one day between slices. Our climate network model then consists of $(N \times S) = 3000$ nodes, where each network node represents a geographical location combined with a delay ranging from 0 to $(S - 1)$ days.
3. **This is the key step, where we apply the structure learning for graphical models**. The network structure, i.e., which nodes are connected by an edge and in which direction, is calculated using the PC algorithm [*Spirtes and Glymour*, 1991] mentioned in the introduction and further elaborated in the supporting information. We use the implementation of the PC algorithm in the TETRAD package (Version 4.3.10-3, available at http://www.phil.cmu.edu/projects/tetrad/) and choose Fisher's Z-test for the conditional independence tests with a significance level of $\alpha = 0.1$. As a priori knowledge we use only that nodes at time t can only have an influence on nodes at the same or a later time. This effectively determines the direction associated with each edge. See the supplemental material for the computational complexity and execution time of this algorithm.
4. Dropping the first time slice of the model proved to be sufficient to deal with the typical initialization problem of temporal Bayesian networks obtained from structure learning, leaving 14 of the original 15 time slices. Furthermore, for this study we decided to also drop all 0 day delay edges, i.e., all instantaneous connections, since we believe they represent the effect of common causes rather than true information flow.
5. The result of Step 4 is a list of all the directed edges in the temporal climate network that spans N physical locations and S different time slices (days). The final step of the procedure is to group all edges with identical start and end point and identical delay time together into *edge groups*. For example, one edge group consists of all the edges that go from grid point 10 to grid point 15 with a delay of exactly 2 days, so we find and count all edges present in the temporal network from grid point 10 to grid point 15 and from time slice 2 to 4, from time slice 3 to 5, from time slice 4 to 6, etc. The number of edges in a group indicates the strength of the corresponding connection.

We define two types of network properties, intralocation properties and interlocation properties [*Ebert-Uphoff and Deng*, 2012b]. Intralocation properties are derived considering only edges between one location's earlier and later instances and are thus measures of "local memory," while interlocation properties consider only edges between different locations and are thus measures of "remote impact". For the present study we discuss only interlocation properties since flow of information across different locations is the focus. Specifically, we use four measures to characterize the information flow in this network. The first is the number of outgoing edges from a specific geographical location ("number of edges" hereafter), which quantifies how actively this location is transmitting information to other locations. The second is the average time delay of the outgoing edges of a location ("average time delay" hereafter), telling us how much further in time the information starting from that location travels as a strong signal. The third corresponds to the average distance of the outgoing edges ("average distance" hereafter) and measures on average how far away the information starting from a location travels as a strong signal. The last measure is the velocity vector of the information flow ("velocity of information flow" hereafter), giving average speed and direction of the outgoing information flow at a specific location.

To detect the signals of climate change as projected by the CCSM4.0 model, we compare these four measures for a climate network derived from the CCSM4.0's 20th century climate simulation against those for a climate network derived from the CCSM4.0's 21st century climate projection. Note that choosing an appropriate significance level, α, is not a trivial task. We used the value $\alpha = 0.1$, which is commonly used in literature. If we increase (decrease) α, the number of edges in the network increases (decreases). However, we found in our past experiments that the overall signal of climate change detected remains the same, so the exact value of α is not critical to the results presented here.

In terms of visualization, we define three different types of plots for each network. *Contour plots* (Figures 1–3) show spatial distributions of selected network properties that have also been averaged over the three grids. *Network plots* (see Figure S1 of the supporting information) show all the interlocation edges of the network for specific delays and for a single grid. An arrow appears in this type of plot whenever the corresponding edge group (see Step 5 above) contains at least one edge. *Information flow plots* also show arrows at grid

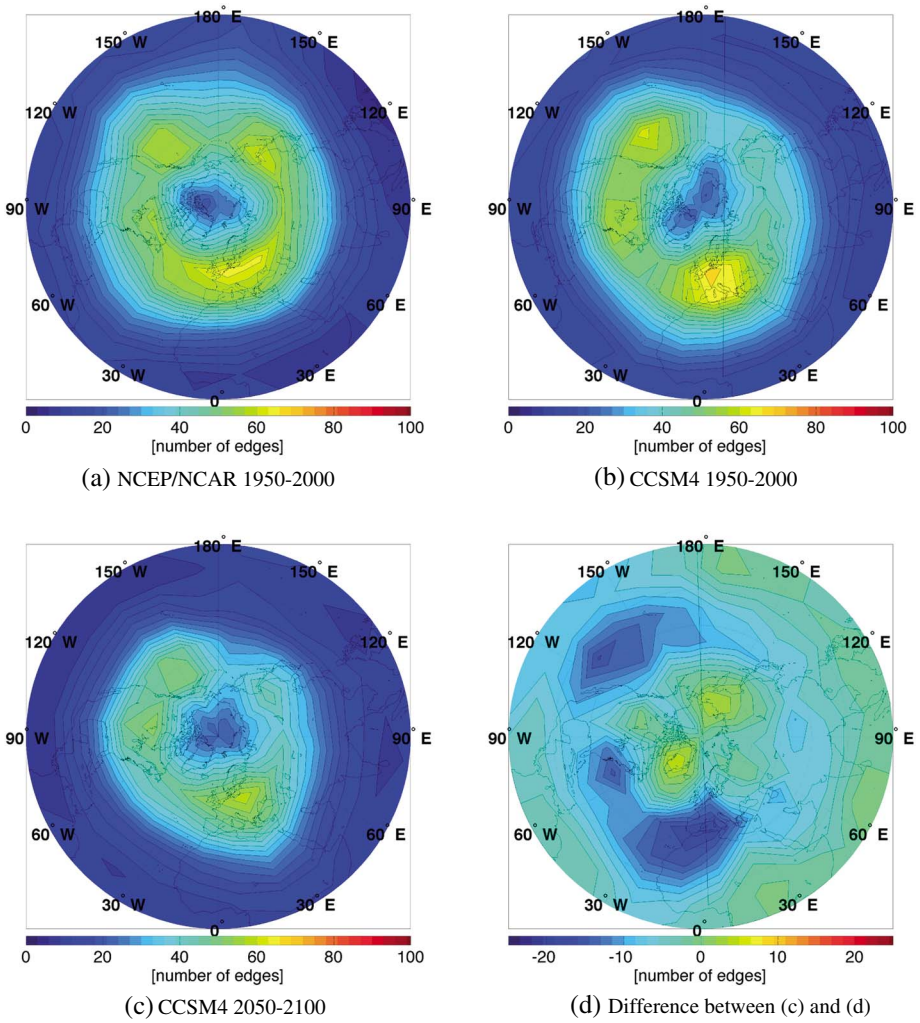

Figure 1. The number of outgoing edges for boreal winter derived from the (a) NCEP/NCAR reanalysis for the period 1950–2000, (b) CCSM4.0's 20th century climate simulation for the period 1950–2000, (c) CCSM4.0's 21st century climate projection for the period 2050–2100. Figure 1d shows the difference between Figures 1c and 1b.

points, but those arrows represent certain information flow properties, such as the average velocity of all outgoing interedges at a grid point (Figure 4). Note that information flow plots, just like network plots, show results for just one grid at a time.

3. Weakening of Atmospheric Information Flow in a Warming Climate in the CCSM4.0

Figure 1 shows the distribution of the first measure, "number of edges" in the NH in boreal winter (December–January–February). Figures 1a and 1b are the results based upon the observational record (i.e., the NCEP/NCAR reanalysis) for the period 1950–2000 and those based upon the CCSM4.0's 20th century climate simulation for the same period. In observation, this field is characterized by local maxima over the extratropical North Pacific and West Europe (Figure 1a). Since "number of edges" quantifies how actively a specific location transmits information to other locations, the local maxima seen in Figure 1a are essentially "information hubs" at 500 hPa level during winter time. The CCSM4.0 model captures the magnitude and general distribution of these information hubs (Figure 1b). Under sustained GHGs forcing and in the late 21st century (2050–2100), the distribution and overall activity level of these information hubs in the model change drastically (Figure 1c). The major differences between the 21st and 20th century model climate include a significant drop of the activity level of the information hubs, particularly over the northern midlatitudes, and a systematic poleward drift of the information hubs (Figure 1d). Since subweekly-scale (synoptic-scale) atmospheric disturbances are the main

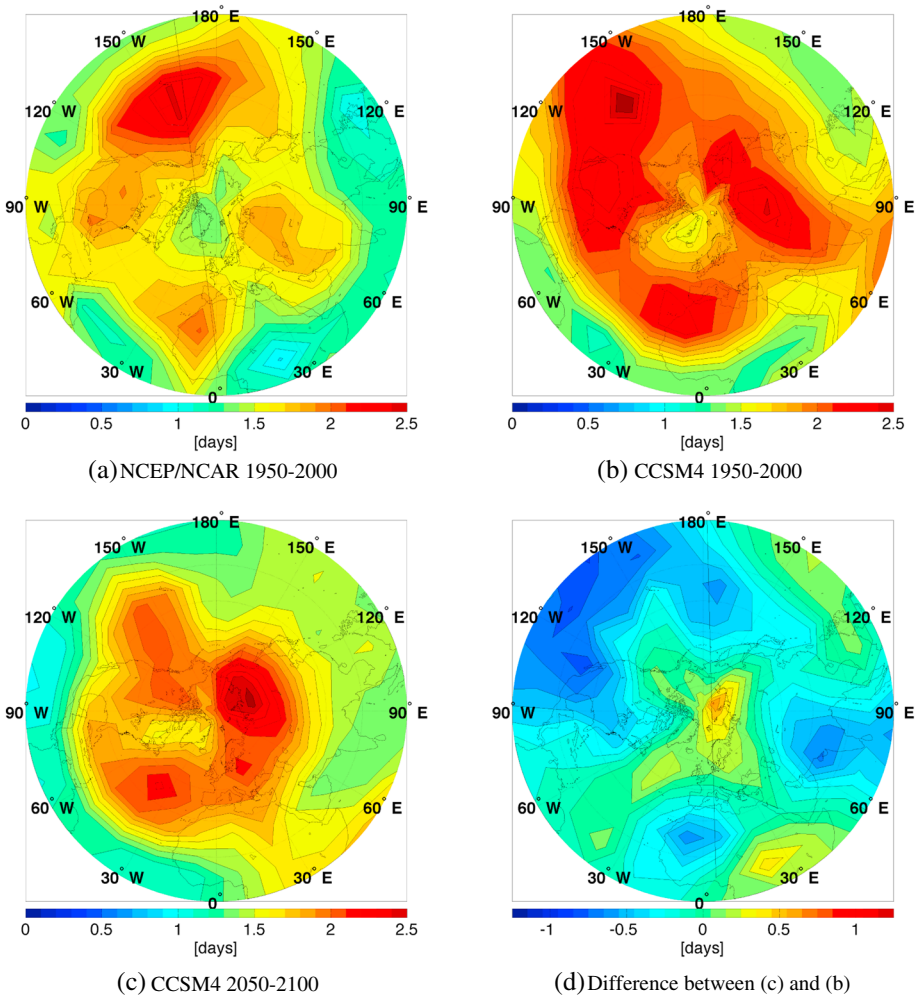

Figure 2. The average time delay (in days) of the outgoing edges for boreal winter derived from the (a) NCEP/NCAR reanalysis for the period 1950–2000, (b) CCSM4.0's 20th century climate simulation for the period 1950–2000, (c) CCSM4.0's 21st century climate projection for the period 2050–2100. Figure 2d shows the difference between Figures 2c and 2b.

information carriers in this system [*Ebert-Uphoff and Deng*, 2012b], the poleward drift discovered here is consistent with findings by earlier modeling studies that the midlatitude storm tracks, i.e., regions of enhanced activity of synoptic-scale disturbances, tend to move poleward as the climate warms [*Yin*, 2005].

Figures 2 and 3 show the counterpart results for "average time delay" and "average distance," respectively. These two measures effective quantify the temporal and spatial extent of the information flow. The CCSM4.0 model is not able to reproduce the distributions of these two network property measures with the same degree of accuracy as it does for the first measure "number of edges" (Figure 2a versus Figure 2b; Figure 3a versus Figure 3b). However, some basic features, such as the concentration of the long-lasting (up to 3 days) and far-reaching (up to 5000 km) information flow in the midlatitudes, are well captured by the model (Figures 2b and 3b). More importantly, the signals of climate change identified through the "average time delay" and "average distance" are consistent with the poleward drift of the main information hubs as revealed by the changing distribution of the "number of edges." For the "average time delay," a general decrease (up to 1 day) of the mean duration of the information flow is found over the northern lower and midlatitudes together with a small increase (up to 0.5 day) in the Arctic (Figure 2d). In terms of the "average distance," there is a reduction up to 2000 km found in the lower and midlatitudes concentrating in the North Pacific and North Indian Ocean (Figure 3d).

Figure 4 plots the last measure — "velocity of information flow". The vector length here corresponds to the average distance across which the information starting from that particular location travels during a 24 h

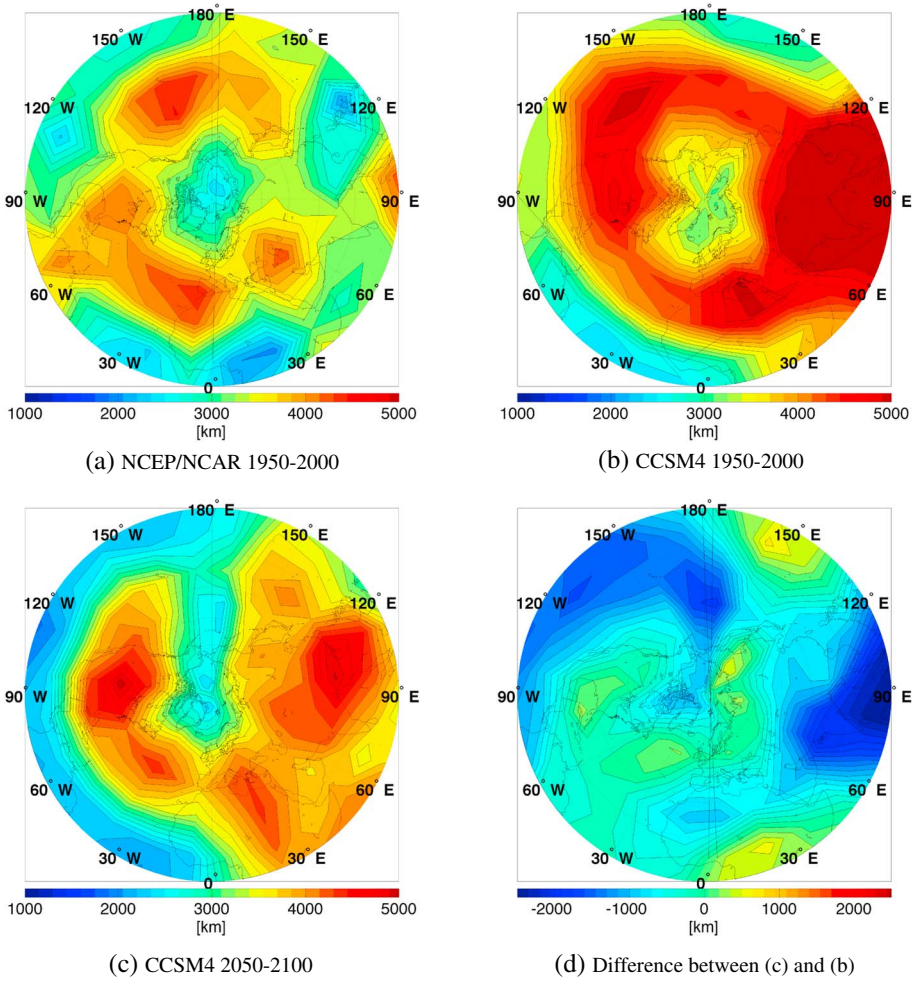

(a) NCEP/NCAR 1950-2000 (b) CCSM4 1950-2000

(c) CCSM4 2050-2100 (d) Difference between (c) and (b)

Figure 3. The average distance (in km) of the outgoing edges for boreal winter derived from the (a) NCEP/NCAR reanalysis for the period 1950–2000, (b) CCSM4.0's 20th century climate simulation for the period 1950–2000, (c) CCSM4.0's 21st century climate projection for the period 2050–2100. Figures 3d shows the difference between Figures 3c and 3b.

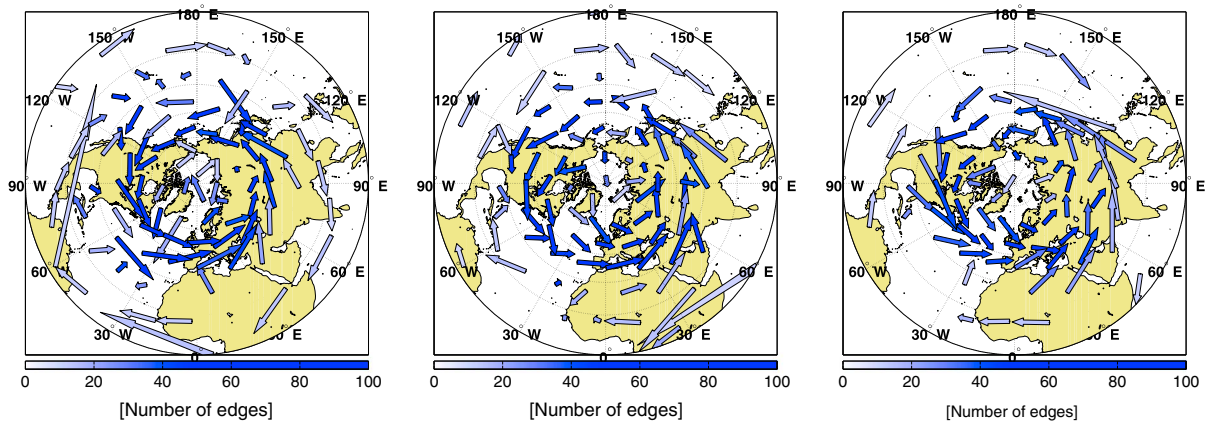

(a) NCEP/NCAR 1950-2000 (b) CCSM4 1950-2000 (c) CCSM4 2050-2100

Figure 4. The average velocity of information flow (in km/day) for boreal winter and Grid 1 derived from the (a) NCEP/NCAR reanalysis for the period 1950–2000, (b) CCSM4.0's 20th century climate simulation for the period 1950–2000, and (c) CCSM4.0's 21st century climate projection for the period 2050–2100. The length of an arrow corresponds to the distance across which the information travels in a 24 h period and color shading of the arrow indicates the overall level of activity of the information pathway (see the main text for more details).

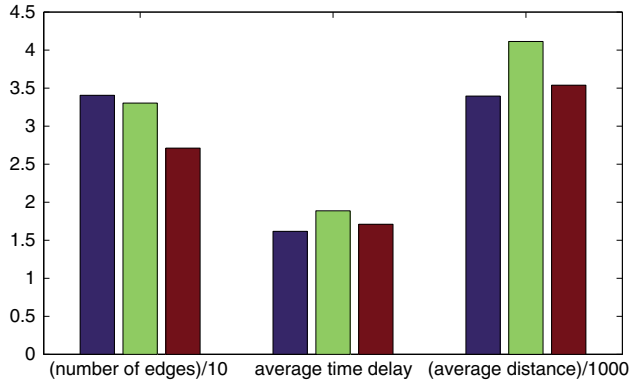

Figure 5. The number, average time delay, and average distance of the outgoing edges averaged over the entire Northern Hemisphere for boreal winter in the NCEP/NCAR reanalysis (blue bars), CCSM4.0's 20th century climate simulation (green bars), and CCSM4.0's 21st century climate projection (brown bars).

period. This distance is calculated for each node of the network considering all out-going edges at that node with lag time of at least 1 day. As outlined in section 2 edges with a lag time of 0 days are likely to be due to common causes and are currently discarded. For each of the edges we know start and end point, as well as time of travel in days, so we can normalize it (taking the curvature of the earth into account) to get the distance vector traveled in just 1 day and then take the average over all such edges at the node, weighted by the number of their occurrence, to get the desired average distance vector. The shading of a vector indicates the level of activity (inferred from "number of edges") of the information pathway represented by the vector. Figure 4a shows the results based upon the NCEP/NCAR reanalysis for the period 1950–2000 while Figure 4b is the counterpart results obtained from the CCSM4.0's simulation of the same period. The model successfully captures the main information pathways in the observation: pronounced eastward-directing information flows that concentrate in the midlatitudes and relatively weak yet very fast westward-directing information flows that prevail in the lower latitudes, particularly over the tropical Pacific and Indian Ocean (Figures 4a and 4b). As projected by the model, in a warmer climate (Figure 4c) the midlatitude information pathways exhibit a tendency of poleward drifting while the lower latitude pathways are diminishing, especially over the tropical Indian and North Atlantic Ocean.

To assess the overall changes on a hemispheric scale, we average the first three network property measures (i.e., "number of edges," "average time delay," and "average distance") over the entire NH and show the averaged values in Figure 5. As demonstrated earlier, CCSM4.0 has the best skill in terms of simulating the "number of edges" — an indicator of the overall level of activity of information hubs. Seen in Figure 5, with enhanced GHGs forcing, the hemispherically averaged activity level drops by approximately 6 units (18%) in the model projected future climate. This drop is accompanied by corresponding decreases in the "average time delay" (by approximately 0.18 days (10%)) and "average distance" (by approximately 570 km (14%)) of the network edges, which indicate, respectively, decreased temporal and spatial extent of the information flow as the climate warms. These changes suggest an overall weakening of the NH midtropospheric information flow in boreal winter in a future climate projected by the CCSM4.0 model. Such weakening tends to lead to reduced interconnectivity thus a more chaotic atmosphere in the near future. A more chaotic atmosphere means reduced intrinsic predictability, which has substantial implications for short-term weather prediction.

Causes of such changes, however, remain partly unclear at this stage. The poleward drift of atmospheric storm tracks in association with enhanced GHGs forcing, as projected by many climate models, could explain the poleward movement of major information hubs and information pathways shown in Figures 1 and 4. The overall decrease of the temporal and spatial extent of the NH atmospheric information flow in a warmer climate (Figure 5) could be contributed by potential changes in the characteristic length and time scales of synoptic-scale disturbances that prove to be the main information carriers in this system. The diminishing of tropical information pathways seen in Figure 4 could be reflecting a suppression of subseasonal atmospheric variability over the tropical oceans due to changes in sea surface temperature distributions and tropical mean atmospheric state as the climate warms. These hypotheses cannot be proved or disproved without a

separate, in-depth analysis of the CCSM4.0 model data. Such an analysis is beyond the scope of the present study, but is on our list of the future tasks.

The causal-discovery-based climate networks constructed here are essentially graphs of information flow in the midtroposphere. Extracting such graphs from reanalysis data and model simulation and comparing the two provide an efficient approach of model evaluation. Compared to the traditional, correlation-based climate networks, graphs of information flow can be more easily tied to actual dynamical processes occurring on relative shorter timescales, making tracing the origin of an identified model deficiency easier. Contrasting properties of information flow between present climate and a warming climate also adds a new way to assess climate change. Graphs of information flow in this sense complements nicely standard metrics used in climate diagnosis. The capability of such a network to reveal key properties of major information pathways in the atmosphere also lays a solid foundation for the development of a probabilistic climate model that incorporates all essential components of the climate system including oceans and lands in the future. In building such probabilistic models, the network analysis done here must be extended to multilevel atmospheric variables such as wind/temperature and surface variables such as sea surface and land surface temperatures to construct first a graph of three-dimensional information flow for the coupled climate system. Finally, we want to stress that the conclusions about weakening atmospheric information flow reached here are based on a single climate model, a single isobaric level data, and considers a specific future emission scenario. The consistency of the conclusion across different models, different atmospheric levels, and the sensitivity of the results to future emission scenarios used are currently being investigated and will be reported later.

Acknowledgments

We thank three anonymous reviewers for their insightful suggestions and comments that led to significant improvement of the manuscript. The NCEP-NCAR reanalysis data used in this study were provided through the NOAA Climate Diagnostics Center and the CCSM4 model output were obtained through the Earth System Grid Gateway at the National Center for Atmospheric Research. This research was supported by the DOE Office of Science Regional and Global Climate Modeling (RGCM) program under Grant DE-SC0005596 and by the NSF Climate and Large-Scale Dynamics (CLD) program under Grant AGS-1147601. We would also like to thank Dr. Tianyu Jiang, at Georgia Tech, for preprocessing the geopotential height data.

The Editor thanks two anonymous reviewers for their assistance in evaluating this paper.

References

Bendito, E., A. Carmona, A. M. Encinas, and J. M. Gesto (2007), Estimation of Fekete points, *J. Comput. Phys.*, *225*, 2354–2376, doi:10.1016/j.jcp.2007.03.017.

Boers, N., B. Bookhagen, N. Marwan, J. Kurths, and J. Marengo (2013), Complex networks identify spatial patterns of extreme rainfall events of the South American Monsoon System, *Geophys. Res. Lett.*, *40*, 4386–4392, doi:10.1002/grl.50681.

Charney, J. G., R. Fjörtoft, and J. Von Neumann (1950), Numerical integration of the barotropic vorticity equation, *Tellus*, *2*, 237–254.

Donges, J., Y. Zou, N. Marwan, and J. Kurths (2009), The backbone of the climate network, *Europhys. Lett.*, *87*, 48007, doi:10.1209/0295-5075/87/48007.

Ebert-Uphoff, I., and Y. Deng (2010), Causal Discovery Methods for Climate Networks, Res. Rep. GT-ME-2010-001, 15 pp., Georgia Institute of Technology, School of Mechanical Engineering, Atlanta. [Available at http://smartech.gatech.edu/handle/1853/36564].

Ebert-Uphoff, I., and Y. Deng (2012a), Causal Discovery for Climate Research Using Graphical Models, *J. Clim.*, *25*, 5648–5665.

Ebert-Uphoff, I., and Y. Deng (2012b), A new type of climate network based on probabilistic graphical models: Results of boreal winter versus summer, *Geophys. Res. Lett.*, *39*, L19701, doi:10.1029/2012GL053269.

Gent, P. R., et al. (2011), The Community Climate System Model Version 4, *J. Clim.*, *24*, 4973–4991.

Gozolchiani, A., K. Yamasako, O. Gazit, and S. Havlin (2008), Pattern of climate network blinking links follows El Niño events, *Europhys. Lett.*, *83*, 28005, doi:10.1209/0295-5075/83/28005.

Hlinka, J., D. Hartman, M. Vejmelka, J. Runge, N. Marwan, J. Kurths, and M. Paluš (2013), Reliability of Inference of Directed Climate Networks Using Conditional Mutual Information, *Entropy*, *15*(6), 2023–2045, doi:10.3390/e15062023.

Holton, J. R., and G. J. Hakim (2012), *An Introduction to Dynamic Meteorology*, 5th ed., pp. 532, Academic Press, Waltham, Mass.

Kalnay, E., et al. (1996), The NCEP / NCAR 40-year reanalysis project, *Bull. Am. Meteorol. Soc.*, *77*, 437–471.

Kistler, R., et al. (2001), The NCEP-NCAR 50-year reanalysis: Monthly means CD-ROM and documentation, *Bull. Am. Meteorol. Soc.*, *82*, 247–267.

Pearl, J. (1988), *Probabilistic Reasoning in Intelligent Systems: Networks of Plausible Inference*, 2nd ed., pp. 552, Morgan Kaufman Pubishers, San Francisco, Calif.

Runge, J., J. Heitzig, N. Marwan, and J. Kurths (2012), Quantifying causal coupling strength: A lag-specific measure for multivariate time series related to transfer entropy, *Phys. Rev., E 86*, 061121.

Spirtes, P., and C. Glymour (1991), An algorithm for fast recovery of sparse causal graphs, *Soc. Sci. Comput. Rev.*, *9*, 62–72.

Spirtes, P., C. Glymour, and R. Scheines (1993), *Causation, Prediction, and Search: Springer Lecture Notes in Statistics*, 1st ed., pp. 526, Springer Verlag, Berlin, Germany.

Steinhaeuser, K., N. V. Chawla, and A. R. Ganguly (2010), Complex networks in climate science: Progress, opportunities and challenges. *Proceedings of the 2010 Conference on Intelligent Data Understanding*, NASA, 16–26.

Tsonis, A., and K. L. Swanson (2008), Topology and predictability of El Niño and La Niña networks, *Phys. Rev. Lett.*, *100*, 228502, doi:10.1103/PhysRevLett.100.228502.

Tsonis, A., and P. J. Roebber (2004), The architecture of the climate network, *Physica A*, *333*, 497–504.

Tsonis, A., K. L. Swanson, and P. J. Roebber (2006), What do networks have to do with climate?, *Bull. Am. Meteorol. Soc.*, *87*, 585–596.

Tsonis, A., K. L. Swanson, and S. Kravtsov (2007), A new dynamical mechanism for major climate shifts, *Geophys. Res. Lett.*, *34*, L13705, doi:10.1029/2007GL030288.

Van Vuuren, D. P., et al. (2011), The representative concentration pathways: An overview, *Clim. Change*, *109*, 5–31.

Yamasaki, K., A. Gozolchiani, and S. Havlin (2008), Climate networks around the globe are significantly affected by El Niño, *Phys. Rev. Lett.*, *100*, 228501.

Yamasaki, K., A. Gozolchiani, and S. Havlin (2009), Climate networks based on phase synchronization track El Niño, *Prog. Theor. Phys.*, *179*(Suppl), 178–188.

Yin, J. H. (2005), A Consistent Poleward Shift of the Storm Tracks in Simulations of 21st Century Climate, *Geophys. Res. Lett.*, *32*, L18701, doi:10.1029/2005GL023684.